Resolution and shape in bioprinting : strategizing towards complex tissue and organ printing

Lee, Jia Min; Ng, Wei Long; Yeong, Wai Yee

2019

Lee, J. M., Ng, W. L., & Yeong, W. Y. (2019). Resolution and shape in bioprinting : strategizing towards complex tissue and organ printing. Applied Physics Reviews, 6(1), 011307-. doi:10.1063/1.5053909

https://hdl.handle.net/10356/105939

https://doi.org/10.1063/1.5053909

Applied Physics Reviews REVIEW scitation.org/journal/are

Resolution and shape in bioprinting: Strategizing towards complex tissue and organ printing

Cite as: Appl. Phys. Rev. 6, 011307 (2019); doi: 10.1063/1.5053909
Submitted: 16 August 2018 · Accepted: 12 February 2019 ·
Published Online: 11 March 2019

Jia Min Lee, Wei Long Ng, and Wai Yee Yeong

AFFILIATIONS

Singapore Centre for 3D Printing, School of Mechanical and Aerospace Engineering, Nanyang Technological University, 50, Nanyang Avenue, Singapore 639798, Singapore

ABSTRACT

In 3D bioprinting, printing resolution represents the deposited material in the x- and y-axes, while dimensionality defines the structural resolution of printed constructs. Dimensionality in 3D bioprinting can be defined as the resolution in the z-axis. The printing resolution, together with dimensionality, contributes to the overall shape fidelity of the bioprinted constructs. The in-depth understanding of physical processes for different printing technologies is imperative in controlling the print resolution and definition. In this article, bioprinting technologies are classified according to the physical processes that deposit or form the bioprinted construct. Due to the different fabrication processes in forming fundamental printed units (voxels), the definition of printability differs for each bioprinting technique. Another aspect of resolution is the spatial positioning of cells within each fundamental building unit. The proximity of cells in the bioprinted construct affects the physiological outcomes. The second aspect of 3D bioprinting technologies is the ability to control shape fidelity. Different strategies have been used to improve the construction of a 3D engineered tissue or organ. Lastly, moving toward complex tissue printing involves adding functionalities to the bioprinted construct. Data processing, material formulations, and integration of different fabrication technologies are key areas in bioprinting that can recapture the different hierarchical aspects of native tissues. This article presents a comprehensive overview of enhancing the resolution of the bioprinting construct and identifying methods to improve functionalities of bioprinted tissues.

TABLE OF CONTENTS

I. DEFINING RESOLUTION AND SHAPE OF PRINT

Lateral resolution (in the x- and y-axes) defines the spatial distribution of materials within each printed layer. Resolution in 3D printing can be determined by the intrinsic feature of the smallest material unit formed (i.e., voxel).[1] In 3D printing, the smallest achievable dimension is determined by printer's input parameters such as the nozzle size, the laser spot size, and the pulse frequency. Print resolution has been reported in terms of the lowest measurable unit of the printed material in the x, y dimensions,[2–5] with lesser focuses on z resolution. The dimensionality of the bioprinted construct can be represented by z resolution in printing. In general, the dimensionality of bioprinting is affected by printing parameters such as the printing path height, path space, and the nozzle diameter which determine the

thickness of each printed layer.[6] A higher number of printed layers increase the likelihood of the deviation from the pre-defined height.[7] Furthermore, material properties such as material contraction/swelling, thixotropy, and the crosslinking mechanism affect the z-resolution. The resolution in the x-, y-, and z- dimensions gives rise to the overall shape of printed structures.

The principle for material deposition is different for each bioprinting technology which affects print resolution and dimensionality differently. To understand the different bioprinting processes, this article discusses about bioprinting technologies in a process-based approach. The classification mirrors and adapts standardized terminologies used for additive manufacturing. As such, bioprinting technologies can be classified as material extrusion, material jetting, and vat photopolymerization.[8]

A. Principles of bioprinting technologies

The fabrication stage of bioprinting is divided into three distinct phases as illustrated in Fig. 1. The three phases are loading (A), printing (B), and structuring (C). The main differences among the different printing technologies lie in the principle and process physics for constructing physical structures from virtual components. In general, nozzle-based technologies such as material extrusion and material jetting move the material along a micro-channel and propel the material towards a build platform. The understanding of jet and droplet formation is essential for material jetting techniques, where the droplet is the fundamental unit which determines the eventual print resolution. The photopolymerization of materials upon exposure to the optical wavelength in vat photopolymerization initiates the printing process. Understanding these basic concepts will facilitate the identification of bio-ink characteristics for printability evaluation.

Due to the intrinsic differences in printing processes, the definition of printability differs across each technology. As such, there is a need to identify process-based requirements for each bioprinting technologies. In general, the definition of printability, as defined by Murphy, is a material's property that facilitates handling and deposition by the bioprinter.[2] It is a term that has been investigated during

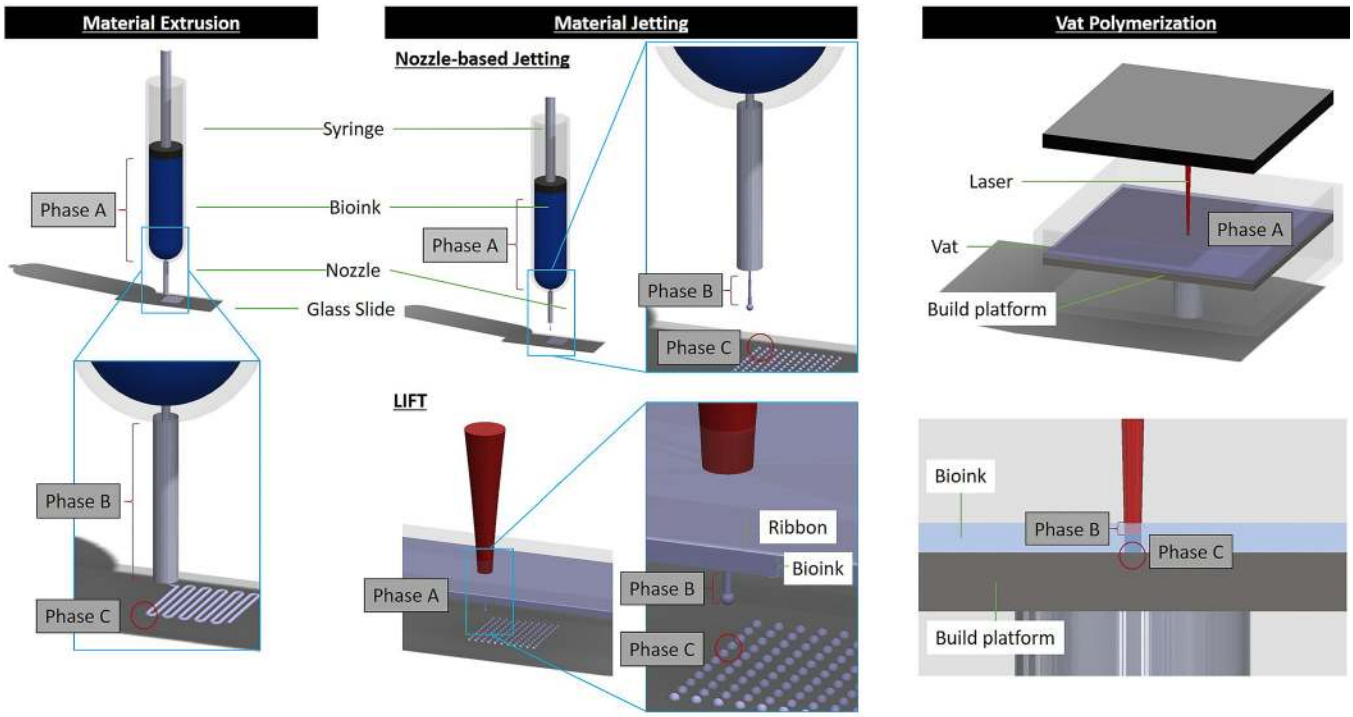

	Material Extrusion	Material Jetting		Vat Polymerization
		Nozzle-based Jetting	LIFT	
Phase A (Loading)	Bioink loaded in syringe	Bioink loaded in syringe	Bioink coated on ribbon	Bioink loaded in vat
Phase B (Printing)	Shearing of bioink in nozzle	Droplet/Jet formation	Droplet/Jet formation	Photopolymerization of bioink
Phase C (Structuring)	Bioink on substrate	Bioink on substrate	Bioink on substrate	Crosslinked bioink within vat

FIG. 1. Setup of different bioprinting technologies highlighting different phases during the bioprinting process. Phase A: Loading of bio-inks onto the bioprinter; Phase B: The bioprinting process; and Phase C: Structuring of the bio-ink on the printing platform/glass slide.

process optimization to have better control over material deposition in bioprinting. The term also encompasses material's rheological properties while extending to the gelation mechanism of different materials. It is essential to balance these parameters to achieve precise and accurate material deposition with desired spatial and temporal control. The printability of a bio-ink is highly dependent on its rheological properties and the use of a suitable bioprinting system. With this definition, it is essential to comprehend that printability is not a term that is limited to certain printing processes. A material can be printable using material extrusion processes whereas deemed inappropriate for material jetting technologies.

As a general guideline for printability assessment, evaluation is conducted using fundamental building units (droplets versus strands/filaments) as the judging criterion for each bioprinting technology. Printability is assessed based on material's properties (e.g., rheology, viscosity, density, opacity, thixotropy, and photo-curing speed) and printer's capabilities (e.g., the nozzle diameter, control of the material flow rate, the printing/scanning speed, and optical fluence). As such, Fig. 2 provides an overview of the different parameters, measurements, and the assessment of material printability according to the printing processes. Section I A begins by understanding the physical processes of technologies. The assessment of printability will be discussed based on the different bioprinting processes.

1. Material jetting

a. Printing process overview. Material jetting is the process in which droplets of the build material are selectively deposited. Technologies such as micro-valve, inkjet printing, and laser-induced forward transfer (LIFT) are examples of the droplet-based deposition technique. For in-depth discussion on the various droplet-based technologies and their applications, readers are referred to the review article.[9] The process of material jetting can be described in three phases: (i) droplet ejection (Fig. 1, Phase B), (ii) pinning of the droplet on substrates, and lastly (iii) spreading of the droplet on substrates. The main difference among the various material jetting technologies is on the actuator used for droplet formation. The process begins with an actuator of thermal, piezoelectric, or laser to induce the instantaneous pressure pulse that propels the ink towards the build platform.[10–14] In microvalve printing, valves are placed at the nozzle to create droplets by regulating the opening and closing frequencies of the valves.[15] The actuator is used to create a rapid cavity volume which translates momentum to eject the droplet of materials. As such, the droplet of ink emerges as a jet which is distinct with a tail like profile (Fig. 3).

The details of droplet dynamics in the inkjet printing process can be found in a recent review.[16] In brief, the inkjet printing process involves transforming pressure waves into kinetic energy and surface energy during the drop formation process. Controlling the jetting process is essential to suppress satellite drop formation where satellite drop formation occurs through (i) misting from the breakup of a secondary tail, (ii) slow and reproducible satellite drops from the pinch-off of the primary tail after head of drop, (iii) fast and reproducible satellites formed through large initial acceleration, and (iv) the Rayleigh breakup of a primary tail. The Rayleigh breaking up of a long primary tail happens when viscous liquids are dropped at high speed.

In laser-induced forward transfer (LIFT), microdroplets are generated when localized heat from the laser beam sublimes a small portion of the ribbon coated with bio-ink, forming a high-temperature and high-pressure vapor pocket.[16,17] The expansion of the vapor pocket results in different types of jets. When a receiving substrate is absent from the setup, the jet eventually breaks into several droplets due to the Rayleigh-Plateau instability.[17] Thus, the reduction of the direct writing height can lead to material deposition onto the substrate.[18] Also, when the laser fluence is above a certain threshold value, the droplet dynamics enters the plume regime, where the vapor pocket is large and overcomes fluid forces, causing the ink to break into multiple droplets.[19] Hence, printer parameters such as the direct writing height and laser fluence are essential in controlling LIFT printing.

b. Ink characterization and printability for material jetting. In material jetting, printability can be assessed through obtaining stable and repeatable droplet ejection.[20] In material jetting techniques, the key properties that influence the ejection of droplets are bio-ink viscosity, surface tension and density, and also the nozzle diameter.[9] Droplet formation follows a series of time-dependent processes which result from a balance between surface energy and viscous dissipation. For Newtonian liquids, dimensionless numbers such as the Reynolds number ($Re = \frac{\rho DV}{\eta}$, ratio between inertial and viscous forces), the Weiber number ($We = \frac{\rho DV^2}{\sigma}$, ratio between kinetic and surface energy), and the Ohnesorge number ($Oh = \frac{We^{\frac{1}{2}}}{Re}$) are useful for understanding droplet formation and jet behavior. The characteristic relaxation time of fluid, λ, is incorporated in the Weissenberg number $Wi = \frac{\lambda V}{D}$ to account for the viscoelastic behavior of non-Newtonian fluid.

In general, the printable range of bio-inks is determined by a dimensionless Z value, which is defined as the ratio between the Reynolds and the Weber number (the Ohnesorge number). Jettability is characterized as an inverse of the Ohnesorge number, capturing relative magnitudes of inertial, viscous, and capillary effects of free-surface fluid mechanics.[21] During the printing process, the droplet velocity is highly dependent on the filament elongation and rupture time.[22] A bio-ink with a lower Z value generally has a slower droplet velocity due to the slow filament elongation and long rupture time and also a higher bio-ink viscosity, hence resulting in lesser droplet spreading.

Droplet formation from viscoelastic fluid involves balancing of inertial, capillary, and viscoelastic forces. The rheological properties of bio-inks affect the filament breakup time and droplet speed, hence forming satellite droplets.[23] Suppressing satellite droplets in the material jetting process ensures printing of a stable and single droplet. To facilitate printing of a higher viscosity material, the pneumatic system is used in micro-valve bioprinting such that tear-off speed is achieved for drop formation.[24] In the nozzle-free setup of LIFT, laser fluence is essential to account for rheological properties such as surface tension and viscosity in jet formation and sustaining cell viability during printing.[25–27] Vapour bubble dynamics in the LIFT system is dependent on the bio-ink's viscosity, where the higher viscosity material results in slower vapor formation.

2. Material extrusion

a. Printing process overview. Material extrusion is a process in which the material is selectively dispensed through a nozzle or orifice. Pneumatic, mechanical piston, and screw extruder are different dispensing variants in material extrusion technology. In the pneumatic

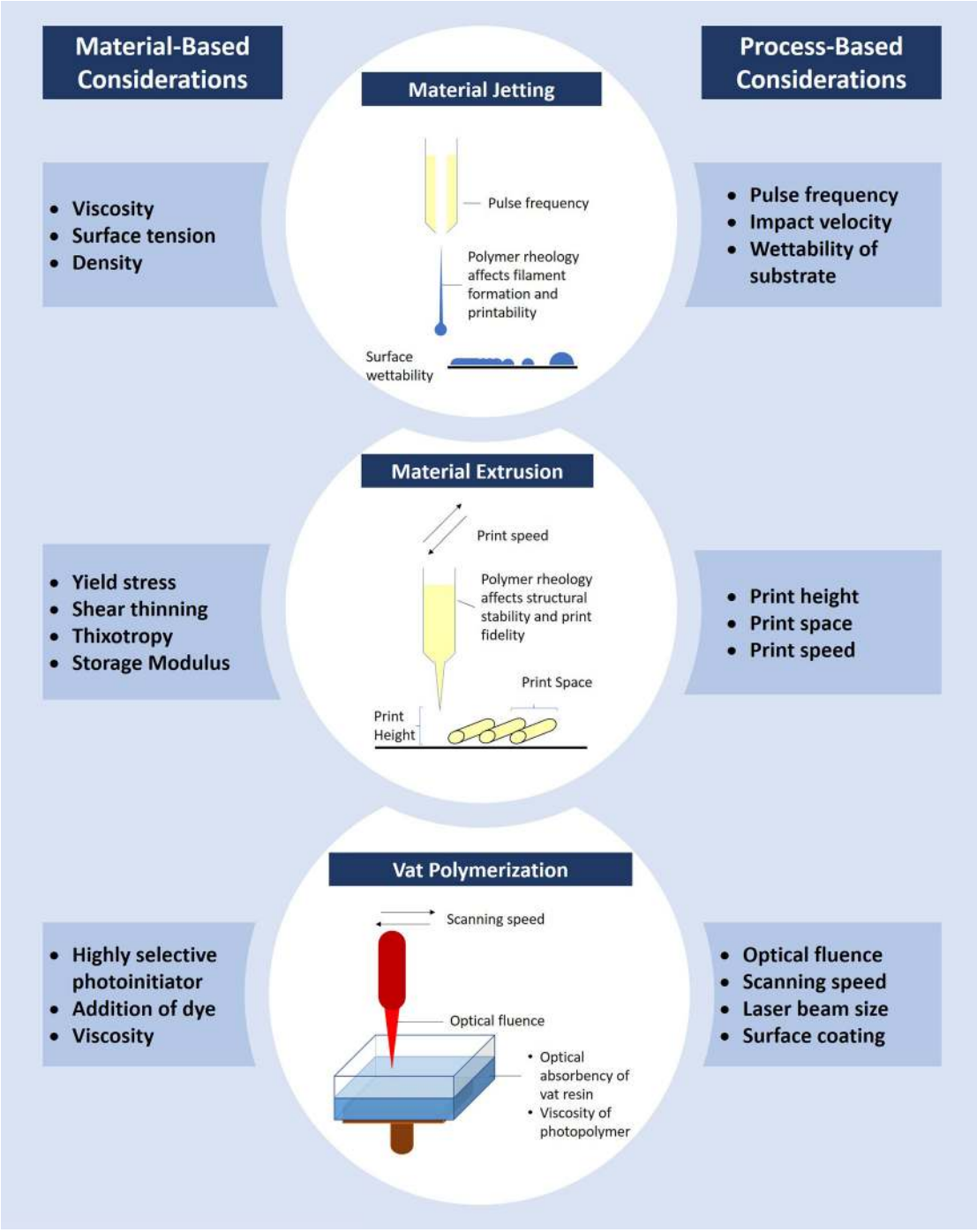

FIG. 2. Material- and process-based considerations affecting printability and print resolution for different bioprinting technologies.

system, pressured air is supplied to a syringe, forcing the material in the syringe to flow through a nozzle. The process performance is affected by fluid flow behavior and air compressibility in a time-pressure dispensing system.[28] The influence of air compressibility is significant when dispensing the material of small amount and results in inconsistent material dispensing as the printing process progresses.[28] In positive-displacement dispensing, a mechanical piston is used to force the fluid through the nozzle when the piston is laterally displaced,

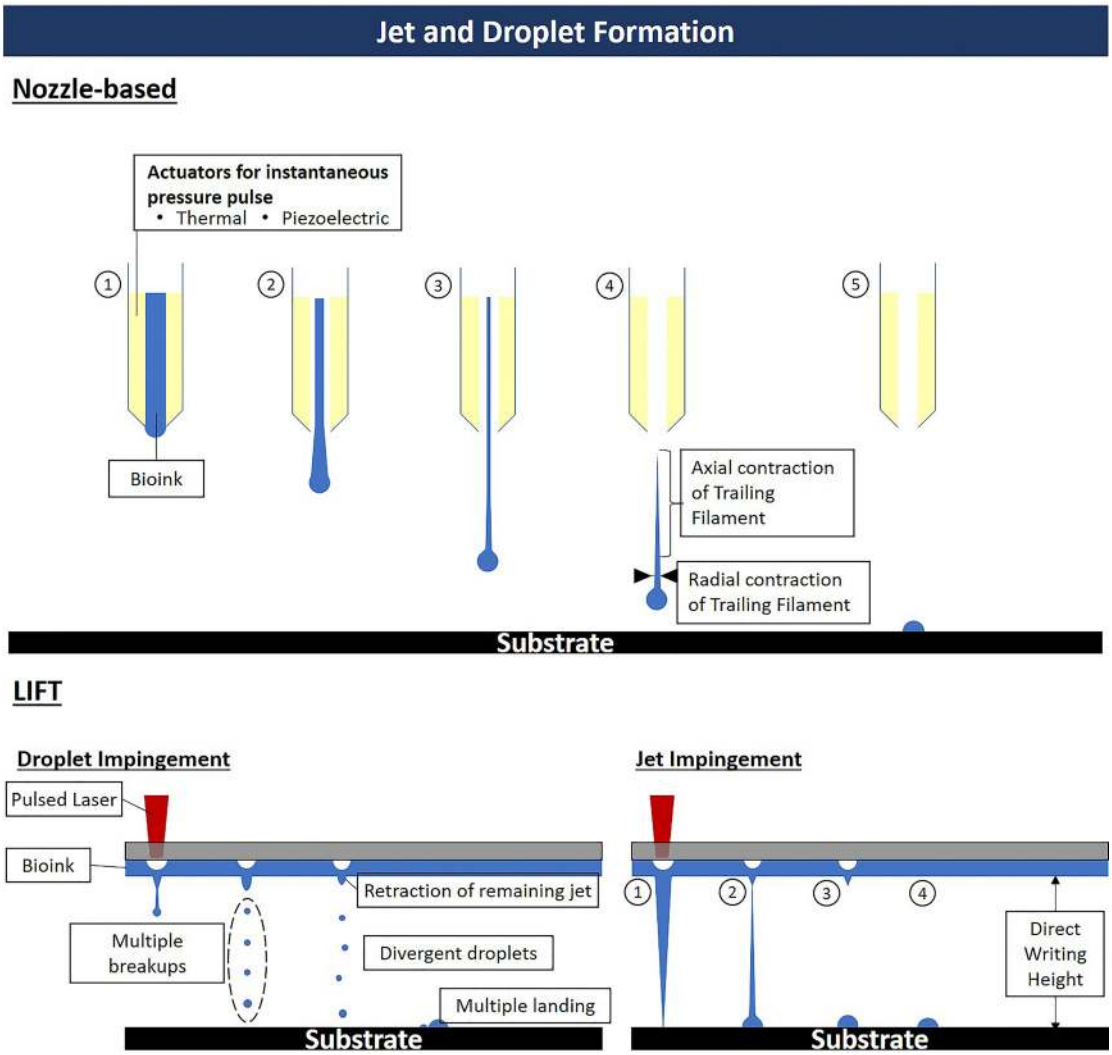

FIG. 3. Material jet and droplet formation distinct with features such as axial contraction and radial contraction of the trailing filament.

whereas in a motor-driven screw extruder, the rotation of the screw moves the fluid out of the nozzle. However, in the screw-based extrusion, high pressure is accumulated at the syringe bottom.[29] As such, pneumatic extrusion[30–39] and positive displacement[40,41] extrusion are the common systems used in cell-laden extrusion-based bioprinting.

The extrusion process can be studied in two regions of the nozzle-based extrusion system (Fig. 1, Phases A and B). An input pressure is needed to move the material along the barrel at Phase A and the fluid flow, eventually narrowing into the nozzle region at Phase B. Different forces acting on the material during extrusion is highlighted in Fig. 4(a). Sectioning the pipe-flow system into distinct regions for analyzing the fluid flow behavior can also be done in the microvalve system with the consideration of geometrical changes within the annulus region.[24]

The material experiences greater shear stress along the syringe barrel at Phase B of the extrusion process.[42] In the extrusion process, cells are affected by hydrostatic forces in the syringe (Phase B) and shear forces in the needle (Phase C). However, hydrostatic pressure less than 500 kPa does not affect the cell viability significantly.[43] As the material flow transits from Phases B to C, the flow narrows and enters the die region (i.e., syringe needle), inducing greater shear stress on the material. The shear stress profile changes at Phase C have a significant impact on the printing performance parameters (Phase C).[42–45]

Different needle geometries induce different shear stress profiles on the bio-ink. A conical needle requires lesser printing pressure, while the average shear stress and maximum shear stress were marginally higher than printing with a straight needle.[42] The needle geometry is a factor that can influence the amount of shear stress acting on cells during printing. Shear stresses in the dispensing needle are the

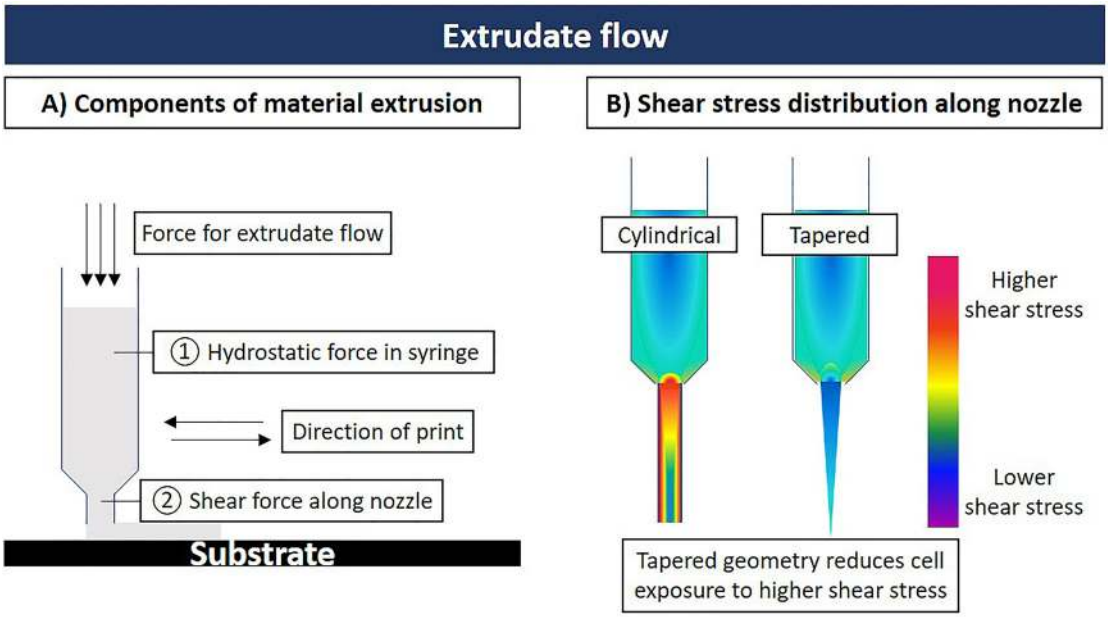

FIG. 4. Material extrusion and shear stress of extrudate flow along nozzle geometry.

contributing factor towards cell viability.[43] In a tapered needle, the geometric feature minimizes the amount of time cells flow through the narrow channel, reducing the detrimental effect of shearing onto the cells.[45] Moreover, the tapered nozzle requires lower pressure when delivering materials of the same flow rate using a straight cylindrical needle.[43,45] The use of a straight cylindrical nozzle generates high shear stresses along the entire nozzle length, whereas by changing the geometry of the nozzle shear, stress peaks only at the nozzle exit, hence improving cell viabilities. Muller reported a maximum shear stress value of 160 Pa that is detrimental to cell viability.[42]

b. Ink characterization and printability. Several rheology models have been used to describe the fluid flow behavior. Common models include the power law and Herschel-Bulkley model.[46–48] Rheological studies are conducted to get material-specific constants (such as flow consistency index, K, and flow behavior index, n) for the understanding of the shear stress condition in the nozzle during printing. To capture the viscoelastic behavior of bio-ink, material characteristics such as λ, relaxation time, are incorporated in the rheological models.[49] Blaeser *et al.* used a combination of the Hagen-Poiseuille equation and power law to describe fluid dynamics for the transient flow of non-Newtonian fluids.[24]

Consensus for assessing printability in material extrusion is to identify material characteristics and printing parameters that extrude the filament/strand.[46,50,51] Materials can be loaded onto syringes and manually extruded to assess on material's printability in extrusion-based processes.[46,47] Paxton *et al.* proposed a two stage evaluation process that assess bio-ink printability, which includes an initial screening step that manually extrudes materials using a plunger syringe.[46] This process helps us to evaluate whether drops or strands are formed before loading the bio-ink to the bioprinter. Other than manual assessment, the consistency measurement using a mechanical tester can be used to quantify the fluctuation of force during bio-ink extrusion.[52] A greater fluctuation in the extrusion force is related to a material of lesser homogeneity, resulting in a less uniform gelation of bio-ink. This assessment helps to select the material composition with homogeneous gel-like consistency. Another form of printability evaluation is to look at cross-patterning of the hydrogel filament. The print outcome is assessed using the image analysis and judged according to the degree of filament merging and blending at a cross-sectional area.[46] Similarly, a printability index, defined as the inverse of the circularity of the enclosed area, was used to characterize hydrogel printed using a cross pattern.[50] To sum up, good printability can be defined by the consistency of the extruded filament diameter.

Rheological evaluation such as shear stress ramping, shear viscosity, and recovery testing was performed to describe ink properties before, during, and after extrusion.[46] The form of the extruded material was characterized as the droplet versus the filament, where the varying degree of gelation affects the morphology of extruded hydrogel.[50] Several studies have used storage and loss modulus to relate with printability. The G' modulus of bio-ink was selected as a criterion for assessing printability based on different degrees of gelation.[50,52] Extrudability, in terms of minimum pressure required, was modeled using G' and G" to assess the printability of bio-ink.[53] Other assessment criteria include checking the uniformity of extruded lines and structural integrity. While the study suggests the loss tangent of values 0.25–0.45 printable, it also highlighted that other rheological properties such as the yield stress may affect printability.

Paxton further showed that consistent inks with distinct filament extrusion have a window period for printing.[46] Crosslinking agents

must be applied within this window period to print additional layers without merging of subsequent hydrogel struts. Combining the shear viscosity measurement, printer's capability, and nozzle geometry, a model is formulated to predict material's printability based on these three factors mentioned.

There are no definite values to determine the printability. However, the assessment on printability can be done prior to printing for the evaluation of bio-ink's suitability for the material extrusion process. Evaluation criteria such as uniformity of printed line and merger of bio-ink filament at cross-sectional point have been used to assess materials' printability for material extrusion processes post-printing. In the attempt to quantify printability, there is a need for uniformity in terms of conducting rheological measurement. A framework or guideline in terms of collecting rheological data will benefit future material development research on printability assessment for material extrusion technology. An index, such as the Z value for material jetting, will be essential to unify the definition of printability for material extrusion techniques.

3. Vat photopolymerization

a. Printing process overview. Vat photopolymerization (VPP) techniques such as stereolithography (SLA), digital light processing (DLP), and two photon polymerization (2PP) fabricate biological constructs through selectively curing a vat of cell-containing photopolymers (Fig. 5).[54–58] The bio-ink consists of photopolymers (monomers and oligomers), photoinitiators, additives (such as inhibitors and dyes), and cells. The bio-ink should be tailored to the printer such that

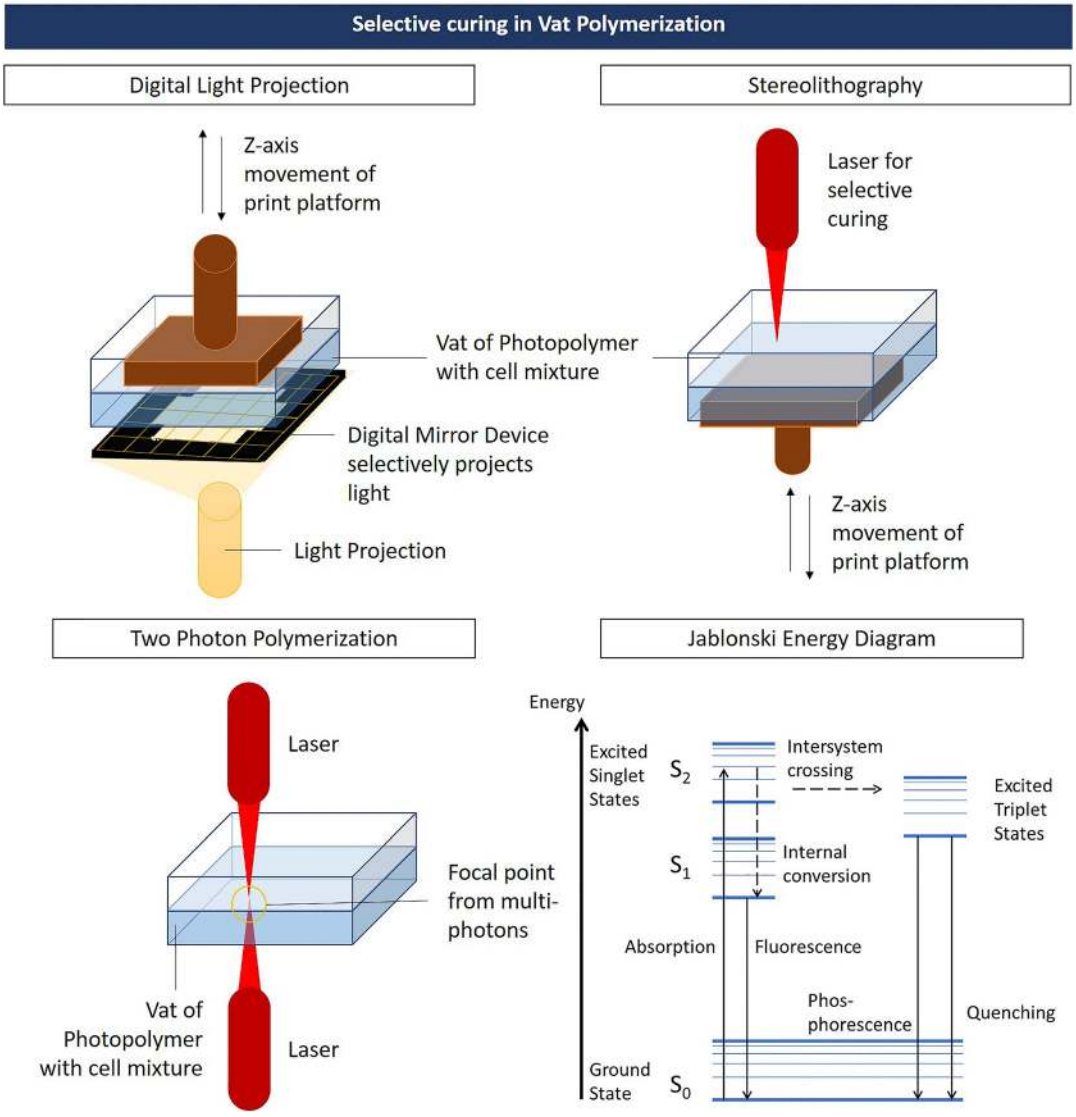

FIG. 5. Schematic diagram of different vat photopolymerization setups showing the differences in curing techniques for each process. The Jablonski energy diagram describes the evolution of molecules in the excited states.

the wavelength and intensity of light source work with the photoinitiators.

VPP systems can be divided into vector- and pixel-based systems.[59] The vector-based approach (SLA and 2PP) fabricates through the exposure of continuous lines that map the contour of each print layer. To form the complete product, the laser hatches across the cross-sectional area. The curing mechanism for 2PP differs from SLA. 2PP requires the incidence of two femtosecond lasers, leading to photopolymerization in the center region of the laser focal spot.[60] For an in-depth review on 2PP, readers are referred to Ref. 61. The pixel-based approach (DLP) fabricates through projecting arrays of light based on the cross-section of a single layer. A major advantage of such system is that the exposure time is independent on the size of the cross-sectional area.[59]

The light-polymer interaction in VPP involves two steps, namely, photophysical and photochemical processes. These processes are described in detail in Ref. 62. In brief, photophysical process is when light is absorbed by chromophores and transits between ground and excited states. Two conditions are critical for light absorption. First, the energy of the photon, $E = h\nu$, must be high enough for the excitation from the ground state to the excited state, ΔE. Second, there must be changes in the dipole moment of the molecule from the incident radiation.[62] The second step is the photochemical process, where the molecules are transformed through cleavage, electron transfer reaction, hydrogen abstraction, etc.

One of the critical parameters in VPP is the cure depth, as described in $C_d = D_p \ln\left(\frac{E_{max}}{E_c}\right)$, where the maximum cure depth C_d is dependent on the penetration depth of the beam D_p, the maximum energy on the resin surface E_{max}, and the critical energy for the ink to change from the liquid to the solid phase E_c. The exposure energy is dependent on factors such as laser power P, laser beam radius w_0, and scanning speed v_s, where $E_{max} = \sqrt{\frac{2}{\pi}}\frac{P}{w_0 v_s}$. In a DLP system, where light projection is used instead of the laser beam, E_{DLP} is used instead of E_{max} when describing the penetration depth.[59] The exposure energy in DLP is dependent on the light intensity of the DLP system I and exposure time t_E, $E_{DLP} = I * t_E$.

In 2PP, the curing process involves the absorption of two photons to excite molecules to a higher singlet state. The probability of excitation by the simultaneous absorption of two photons is quadratically related to the incident light intensity. Thus, submicron resolution can be achieved using 2PP, while structures can be printed with a greater depth and at faster speed.[62] However, multiple curing mechanisms can occur in the 2PP system other than two photon absorption. Avalanche ionization, where a region of highly intense electric fields causes insulating species to be conductive, and polymerization through heating are other curing mechanisms in 2PP.[61] For in-depth readings on 2PP using near-infrared radiation for biological applications, readers are referred to a recent review article.[61]

b. Ink characterization and printability in vat photopolymerization. Printability in vat photopolymerization has been less studied as compared to the other two processes. Nonetheless, printability can be defined by decoupling the processing components in vat photopolymerization. The main advantage in VPP is that the ink need not be tailored to physiochemical properties such as surface tension, viscosity, and volatility.[63] The effect of photopolymer's viscosity is essential when refilling the vat.[64] Higher viscosity ink will require a longer time to reach equilibrium during the recoating process due to surface tension.[62]

The light absorbency of resin influences the area at which photopolymerization occurs in the vat system. Dyes can be added to the photopolymer resin to absorb scattered light from the light projector.[65] Agents can be added to limit light penetration in vat photopolymerization such that good z-resolution can be maintained.[66,67] Photo-absorbers improve print resolution through limiting the light penetration depth, preventing unwanted curing of the bio-ink.[68] Another aspect of the bio-ink for VPP is on the choice of photo-initiators. The photo-initiator has to be highly selective upon activation to prevent unnecessary free radical crosslinking, resulting in the polymerization of larger volume.[69]

B. Resolution of materials and cells within bio-ink

1. Print resolution as a function of printer's parameters

Most bio-inks for nozzle-based jetting are Newtonian fluid with low viscosity, where the viscosity does not change with the shear rate.[70,71] For material jetting, it is important to achieve the formation of a distinct single droplet. Several approaches can be used to modulate the droplet size, while using the same printhead and ink. First, the pulse width between fill-before-fire can be adjusted to control the drop size.[16] Also, the interaction of the droplet on the substrate influences the droplet resolution. A substrate surface with higher contact angles would result in smaller droplet spreading due to slow energy dissipation.[72] A higher impact velocity leads to an increase in the maximum energy available for droplet rebound. The spreading of droplet on the substrate is influenced by surface tension and viscosity.[73]

Bioprinting with dimensionality in droplet-based printing involves the coalescence of neighboring droplets. Droplet spacing influences the coalescence morphology, forming either individual drops, scallop lines, or linear lines.[73] To create lines and areas of print requires the connection of individual adjacent droplets. The high Laplace pressure generated between two touching drops results in fast flow towards the connecting region.[16] Additionally, the height difference between the receiving substrate and printhead influences the size of printed droplets.[74,75] By controlling the print height, secondary droplets can be suppressed, and thus, ensuring that only primary droplets are produced.

Other than material's characteristics, printing parameters such as printing pressure, path-height, path-space, and nozzle moving influence the print outcome.[7,47,76,77] The printing pressure affects the length, width, and height of printed layers.[6] When a low pressure is applied, the pressure is insufficient to extrude the bio-ink immediately and leads to either a no print or an underprint. In contrast, a higher pressure induces rapid bio-ink extrusion and also overprint and excess bio-ink spreading along the width.[6] The path-height affects the length and height of the printed layers when (i) the nozzle causes disturbance to printed layers while traversing at a lower path height and (ii) extruded bio-ink cannot reach the building platform on time at a higher path height. An optimal path-height is approximately 75% of the nozzle diameter (normalized path-height). A change in nozzle moving speed has little effect on the printing outcome, and the effect is only significant when the viscosity of the bio-ink is low.[76]

In stereolithography, printing parameters such as print speed, laser beam size, and optical fluence are parameters that affect the print resolution and accuracy. Print resolution for stereolithography was reported to be less than 100 μm.[69,78] Improved print resolution is achieved through increasing the stage velocity and reducing the optical power of the laser.[69] With higher scanning speed and lower optical power, there is lesser area exposed to sufficient optical fluence. Thus, the higher print resolution is produced. An optical fluence model is used to describe the hydrogel line width as a function of peak optical fluence, where there is a threshold optical fluence that is necessary to initiate photo-crosslinking.[69] The surface of vat can be coated to minimize the meniscus formation of the photopolymer for ensuring complete polymerization, hence improving the shape and thickness of polymerized construct.[79]

2. Print resolution as a function of the cell concentration

Another factor that influences print resolution in general is the cells within bio-ink. It is notable that cells do occupy volume within the bio-ink mixture. With the increasing cell density, the proportion of cells within bio-ink increases and hence affects the properties such as viscosity and rate of gelation. At temperature above the gelation point, bio-ink with a loading cell density of 1.5×10^6 cells ml^{-1} decreases in viscosity by a factor of 2, and the factor increases with the increasing cell density.[31] The presence of cells increased the storage modulus of the bio-ink and is attributed to the viscosity changes. The cell density also influences the time required for the gelation of bio-ink. It was shown that for NIH 3T3 and HepG2 C3A cells, a threshold value of 25×10^6 cells ml^{-1} will determine the gelation rate of the bio-ink.[40] Skardal also reported that the threshold value in which cell density interferes with hydrogel formation is cell-type specific.

The effect of the cell concentration has an impact on droplet formation and thus the print resolution. The increasing cell concentration delays the necking of the ligament which prolongs the breakup time.[80] Also, the addition of cells increased viscous and elastic effects and thus suppressed the formation of satellite droplets. With the increasing cell concentration, the viscosity increases and the surface tension decreases, resulting in an overall decrease in Z values. As shown in the fluorescent microscopy images in Figure 6, once the Z values drop below a threshold level, the cell-laden bio-inks become unprintable.

3. Resolution of cells within print

There are 2 main types of cell-laden bio-inks, namely, cell-encapsulated hydrogels and cell suspension.[81,82] As shown in the fluorescent microscopy images of Figure 6, cell distribution within each fundamental unit (filaments in material extrusion and droplets in material jetting) is randomized. One of the challenges in bioprinting is the inability to spatially localised positioning of cells and hence the deviation of cell density within each deposited unit.[71,83] The lack of control over cell distribution is prevalent in the pre-printing stage, which affects the printing output over time.[84]

The key challenge is to ensure cell homogeneity in cell-laden bio-inks during the bioprinting process; gravitational forces induce cell sedimentation which resulted in non-uniform cell distribution within the bio-ink over time. Recent works have highlighted the influence of cell sedimentation which resulted in inconsistent printing output over time.[84,85] It was observed that cell sedimentation caused an initial increase in cell output over the first 15 min of printing until it reached a plateau, followed by a reduction in cell output over time.[84] Although the mathematical model has predicted a linear increase in cell output over time before reaching a constant steady-state output, the experimental results do not corroborate the numerical simulations. This is mainly due to cell adhesion along the constriction of the printing cartridge that occurred because of the presence of van der Waals interactions between the cells and the interior surface of the printing cartridge.[86,87]

A counteractive approach is to modify bio-ink formulation to include non-adhesive polymers[71] or weakly crosslinked hydrogel[88] in order to reduce the effect of cell sedimentation and adhesion. Some of the previous studies attempted to mitigate this cell sedimentation effect by incorporating ethylene diamine tetra-acetic acid (EDTA) within the bio-inks[89] and achieving a state of neutral buoyancy between the encapsulated cells and bio-inks.[90] A recent study has incorporated polyvinylpyrrolidone (PVP) molecules within the cell suspension, where the PVP-based bio-inks improved the cell viability and homogeneity during the printing process.[71]

Other than bio-ink modification to improve the cell distribution, mechanical inputs can be designed into the bioprinting system to aid in cell positioning. One such technology is surface acoustic waves (SAWs). In the earlier work on SAWs, the technology was used to encapsulate cells in each ejected picolitre droplet with a high cell viability of >89.8% at high throughout rates of up to 10 000 droplets per second.[91] It is challenging to precisely control the number of ejected cells using the SAW approach; the number of cells per ejected droplet is mainly determined by the cell concentration in the ejection fluid and by the ratio of droplet size to cell size. Particularly, a low cell concentration of 1×10^6 cells/ml would result in up to 24.4% empty droplets, whereas a high cell concentration of 16×10^6 cells/ml would result in up to 1.6% empty droplets.

Other than the use of acoustic waves as droplet generators, SAWs were used to control the positioning of cells to decrease the cell proximity within the encapsulating material. The alignment of particles relies on the incident wave and the distribution of forces on the object. The positioning effect of the cell using SAW is dependent on cell properties such as size, compressibility, density, and material's fluidic properties such as viscosity. Enhancing the cell-cell contact is critical in tissue development and function.[92]

II. STRATEGIES IN ENHANCING SHAPE FIDELITY IN CELL-HYDROGEL BIOPRINTING

A. Formulation of superior bio-ink

Hydrogel precursors are considered too liquid for printing applications, whereas crosslinked hydrogels are too brittle to be extruded through a needle without fracture.[93] The storage modulus and viscosity indicate whether a material can be self-supporting, whereas viscosity recovery after shear shows whether cells can be incorporated within the bio-ink.[93] The formulation of bio-ink that comprises multiple hydrogels is a commonly used approach to enhance the structural integrity of bioprinted constructs.[51,94–100]

The mixture comprises a primary material that improves printability and shape fidelity during printing, while the secondary material later undergoes crosslinking to provide structural fidelity after printing.[30,39,51] For instance, the gelatin methacrylamide (GelMA)/

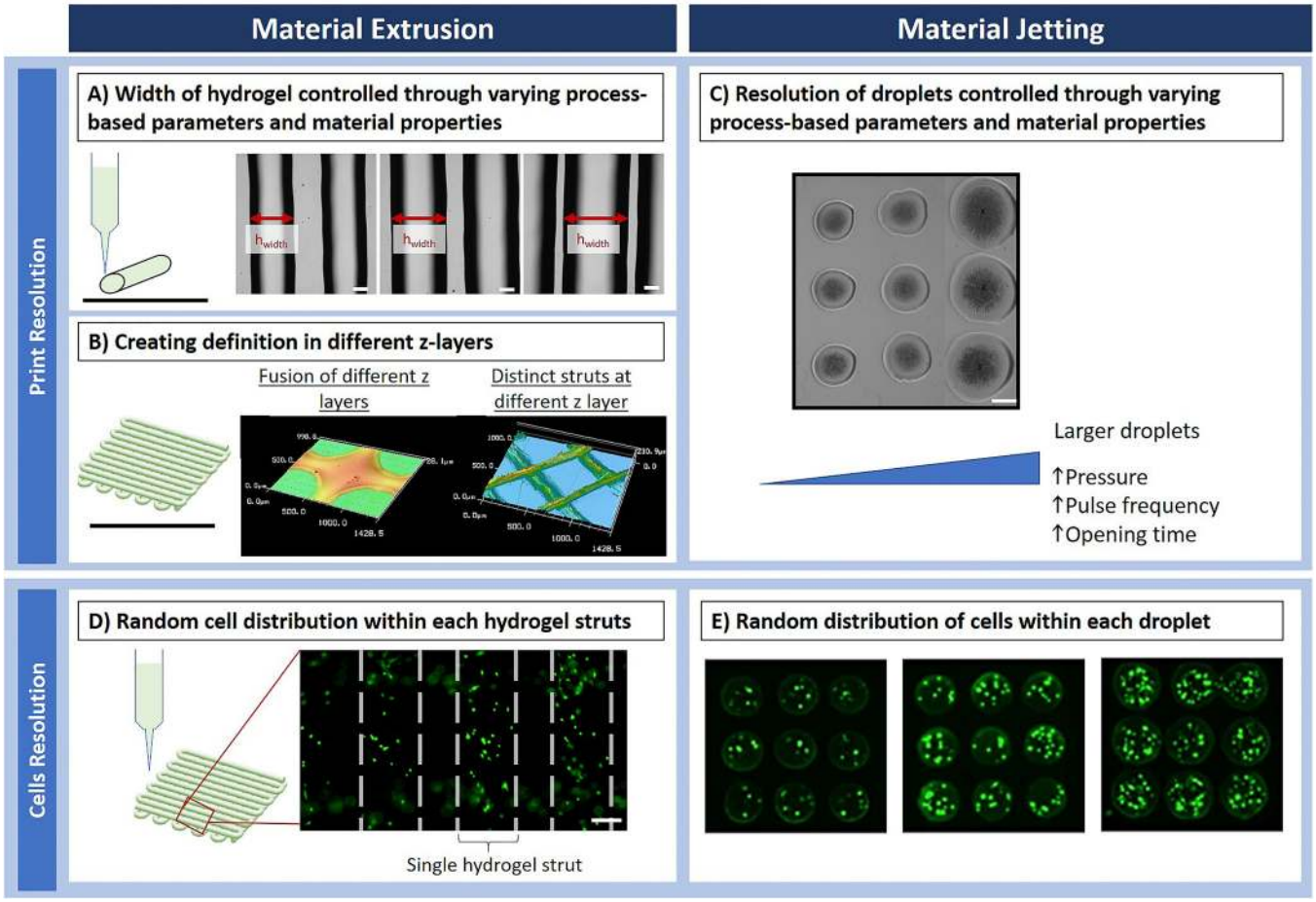

FIG. 6. Print resolution and cell resolution of the bioprinted construct shown using material extrusion and material jetting techniques. The print resolution of both material extrusion (a) and (b) and jetting (c) controlled using material- and process-based parameters. The microscopy images of struts and droplets showed variations in print resolution while improving on the print definition (b). Random cell distribution shown within struts (d) and droplets[71] (e).

hyaluronic acid (HA) mixture showed enhanced printability as opposed to using GelMA alone.[51] HA improves the viscosity of the mixture, while the crosslinking of GelMA retains the structure's integrity after printing. In the investigation with varying molecular weights of PEG, hydrogel with longer polymer chains exhibited higher stretchability.[95] The dual hydrogel system comprising an interpenetrating network of PEG with sodium alginate displayed an increase in fracture energies when reversible Ca^{2+} was added to the system. Alternatively, partial gelation can be performed on hydrogel with the multiple crosslinking mechanism to enhance the viscosity of bio-ink. One such example is to induce thermal gelation in GelMA through lowering of temperature.[44]

On the other hand, a single component hydrogel system is ideal for cell printing without the added complexity from bio-ink mixed with multiple hydrogels. Increasing the number of hydrogel in the system adds complexity in terms of satisfying environmental conditions during bioprinting. The multi-network hydrogel system is sensitive to more than one external stimulus (e.g., light, temperature, and ion concentration). As such, polymers are synthesized to improve the mechanical strength and elasticity.[101] Another approach to the single component hydrogel system is through mixing of the modified and pristine materials. For instance, when carboxylated agarose is mixed with pristine agarose, the elastic modulus of printed gels was enhanced while keeping the shear viscosity relatively constant.[102] This is essential when printing technologies require a smaller range of viscosities such as microvalve and inkjet printing.

Another approach to improve on bio-ink formulation is the addition of nano/microparticles to enhance bio-ink's mechanical functionality. Nanoclay particles are used to improve the viscosity of the pre-gel solution while increasing its shear thinning properties.[93,95,103] The thixotropic response time for such a colloidal system is reported to be on the order of 0.1 s, deeming these nanoparticle-based bio-ink as versatile self-supporting scaffold materials.[103]

Silk fibroin (SF) particles were added to gelatin methacrylate (GelMA) to increase the viscosity of bio-ink while reducing the cell sedimentation effects.[100] SF microparticles were formed through sonication, which accelerated the crystallization process. The addition of SF increased the viscosity of bio-ink to 140 folds. Cell dispersion in the

bio-ink was improved with a higher SF content. However, an excess amount of SF particles induces rapid gelation, decreasing the printability of bio-ink.

Other than viscosity modifiers, micro-carriers can be designed to deliver either cells or biological factors. Nanospheres loaded with growth factors are mixed with the bio-ink for sustained, slow release of stimulating factors in promoting cell growth.[104] Single cell encapsulation using flow focuses the droplet-based microfluidic platform to coat cells with microgels of sizes less than 50 μm.[105] These microgels act as immune-protective barriers that prevent the exposure of encapsulated cells to host's immunoglobins. Such modular bio-inks allow the delivery of non-autologous cells for stem cell therapies while providing host-centric macroenvironments. Moreover, micro-carriers can be used as devices that aid in expansion of cells prior to printing while reinforcing the mechanical integrity of the soft matrix.[106]

B. In-process crosslinking

Hydrogel with the rapid gelation mechanism, such as alginate and fibrin, is commonly used during the in-process crosslinking method[107,108] . In-process crosslinking is achieved by either modifying the extrusion head for coaxial extrusion of the hydrogel precursor and crosslinker or depositing the precursor into the crosslinker bath.[108–110] Another approach is to setup peripheral crosslinking devices that induce targets curing the process just before landing on the substrate.[110]

Alternatively, the precursor hydrogel and crosslinker are sequentially deposited via designing the printer's toolpath.[111–114] Sequential deposition is prevalent in material jetting techniques, where low viscosity solutions are needed for smooth jetting. Sodium alginate is one of such quick gelation polymer solution with low viscosity. Another example of rapid crosslinking involves the use of horseradish peroxidase (HRP)-catalyzed hydrogelation.[115] This gelation mechanism targets polymers with phenolic hydroxyl (Ph) moieties. The mechanism for this crosslinking technique is to target phenolic groups that have been added to the natural polymer for initiating the enzymatic crosslinking reaction.[116–118]

C. Support-enabled approach

Hydrogel, being a soft material, has limited capabilities in supporting its structure. Two deposition strategies have been used in the build/support configuration. First, the support material can exist as the bath where the print is embedded within the vat comprising materials not restricted to hydrogels alone,[119–123] whereas support materials can be deposited sequentially with build materials.[124–130] Build materials refer to the intended engineered tissue component (i.e., cells and/or hydrogel), while support materials provide mechanical strength to hold the structure. In most cases, the support material is removed through post processing.

Previously, high density fluorocarbon was used to support lesser buoyant and soft hydrogels.[121] Upon comparing printing agarose in air and in fluorocarbon support bath, a 28 mm hydrogel rod with an aspect ratio of 17.5 was printed uniformly, whereas the agarose rod printed in air collapsed after a critical height has been reached. Bioprinting in air versus into another medium (e.g., oil bath) affects also the resolution of print.[122] The droplet of cells that were printed into the oil packed into an hexagonal array and the construct was stabilized with agarose. The addition of Fmoc-dipeptides increases the interfacial adhesion between printed droplets, hence improving shape retention. Printing into a support bath overcomes the limits of gravitational force.[101] This approach to print soft hydrogel into a bath other than air is one of the strategies used in build/support printing to improve on structure retention and shape fidelity. The hydrogel crosslinker can be incorporated into the support bath to enhance print fidelity, while the sacrificial bath is removed.[119] Hydrogels with the reversible crosslinking mechanism such as gelatin, Pluronic F127, and agarose are commonly used as the support material. Sacrificial ink 30% w/w Kolliphor P407 was used.[131] The removal of the sacrificial mold is induced through washing with cooled water.

The use of computer-assisted technology in bioprinting allows integration with other fabrication processes. For instance, bioprinting techniques (such as extrusion and inkjet) have been integrated with melt-plotting and electrospinning apparatus to build multiscale parts.[13,34,36,128,132–134] Thermoplastic PCL and poly (lactic-co-glycolic acid) (PLGA) are commonly used as the support material for hydrogel in hybrid printing. These thermoplastics are processed at high temperature which is not compatible to include cells in the plotting process. Instead, cells are deposited onto the thermoplastic using hydrogel as the carrier (Table I).

III. TOWARDS COMPLEX TISSUE AND ORGAN FABRICATION

Anatomical geometries with controlled accuracy can be three-dimensionally bioprinted with recent studies showing the capabilities of printing virtually any anatomical designs.[39,41,119,137,138] Going beyond recapturing the shape and form of the native tissue/organ, there is a need to recreate the highly complex hierarchical structures found in native human tissues and/or organs.[2,139] With print resolution limited in the micrometer range, incorporating other fabrication modalities with bioprinting proves to be a disruptive approach in recapturing the multi-scale heterogeneity of complex tissues/organs. The modification in the following aspects of bioprinting enhances the functionality of the bioprinted construct.

A. Data processing for the voxel-based biofabrication of complex tissue

Constructs with anatomical resemblance have been bioprinted using data from either medical imaging or manually designed using CAD software.[39,138] The ability to print any virtual shapes renders bioprinting a technology for producing the anatomically accurate 3D construct to mimic the targeted tissue or organ. STL is the commonly used file format for providing the blueprint to print. As STL file formats are boundary representations of the virtual bodies, objects are represented by the list of triangles and vertices, with the inner space bounded by the triangles occupied by a single material. This can be described as a shell only representation. With printers capable of printing up to 7 materials, objects that are not naturally represented as the surface has to be converted to boundary representation.[140] Voxel-based blueprints that contain point-specific attributes are essential for more accurate representation.

Multi-material printing is a distinct advantage of bioprinting which many has leveraged on to produce better engineered tissue through printing.[124–130] Recent advances in the use of the microfluidic platform with 7 channels showed heterogeneous printing for recapturing different aspects of the native tissue.[141] By digitally tuning valves

TABLE I. Strategies to enhance shape fidelity in cell-hydrogel bioprinting.

Strategies	Description	Bioprinting techniques		References
Formulation of superior bio-ink	Bio-ink with the multiple hydrogel system for enhancing rheological and mechanical properties	Extrusion		30,39,44,51,94–99
		DLP		100
	Synthesis of bio-ink through the co-polymer for single component hydrogel system	Extrusion		101,102,135
	Nano/microparticles to enhance the mechanical functionality	Extrusion		93,95,103
		DLP		100
In-process crosslinking	Modification of printhead	Extrusion		108,110
	Induce crosslinking upon printing through the designing of the toolpath	Extrusion		113,119
		Material Jetting	Inkjet	109,115
			Microvalve	111,112,114
	Induce crosslinking upon landing on the print substrate through peripheral devices	Extrusion		110
Support-enabled approach	Printing of bio-ink into the alternative medium other than air (e.g., support bath, mold, and higher density liquid bath)	Extrusion		119,120,124,125
		Inkjet		13,122,126
	Hybrid technology for the fabrication of the scaffolding material and bioprinting	Extrusion		34,128,134
		Inkjet		136

that direct different materials, continuous microfiber with spatial coding is extruded through a single printhead. As such, voxel-based printing coupled with continuous fabrication of filamentous bioprinted materials can potentially support the heterogeneous printing of native-relevance tissues.

Print accuracy from obtaining blueprints of medical imaging requires further optimization. When obtaining print data from medical imaging, the process involves two major steps concerning data acquisition and data conversion. As such, the print accuracy of the reconstructed file from medical images is influenced by factors such as resolution of the acquisition technique and printers' capabilities. Different imaging techniques have different resolutions when collecting data, where the axial resolution of OCT is at 5–7 μm and the CT scan resolution is limited at 100 μm. Overall, there is a limit towards how much details can be represented in the reconstructed construct.[142] On the other hand, it is inevitable to have geometrical differences between printed and intended dimensions.[1] Hence, when bioprinting constructs from reconstructed medical imaging, deviations in terms of data acquisition, conversion, and print have to be accounted.

B. Enhancing functionalities through material formulation

Electrically conductive polymers have gained attention tissue engineering applications such as nerve and cardiac.[143,144] For instance, adding conductive elements to bio-ink creates a proper microenvironment for the organization of cardiac cells.[141] Gelatin methacryloyl mixed with gold nanoparticles was incorporated with cardiac fibroblasts (CFs) and cardiac muscle cells (CMs). Gold nanoparticles increased the electrical conductivity of the hydrogel material, which enhanced the cell-cell connection. The gold nanoparticles improve on electrical conductivity of the bio-ink, and also serve as modulators for balancing the ratio between CFs and CMs.[145]

Designing smart hydrogels that are programmed to respond to external stimuli can increase the functionalities of the bio-ink system through inducing preferential changes of the bioprinted construct. Smart hydrogels can be used to manipulate the network structure and swelling ratio using external stimuli such as pH and electrical or even magnetic fields.[146] Patterning hydrogels with soft regions in stiff hydrogel with photolabile moieties.[147] Alternatively, the selective erosion of the material can be achieved through patterning of photolabile group that is sensitive to a specific wavelength.

C. Controlling material deformation through bioprinting

Mechanical deformation during the bioprinting process can influence the behavior of both cells and materials. The shear-induced alignment of anisotropic particles through extrusion printing was printed to align anisotropic particles. A recent study has developed a biomimetic hydrogel composite (stiff cellulose fibrils embedded in a soft acrylamide matrix) that can be 4D printed into a programmable bilayer architecture.[148] Extrusion printing aligns the anisotropic cellulose fibrils, leading to the anisotropic stiffness of the printed construct. The structure was encoded with localized swelling anisotropy that induces complex shape changes upon immersion in water.

Shearing in bioprinting was used to induce transient membrane permeability for *in situ* cell reprogramming.[149] Fibroblasts that experienced the extrusion method were analyzed for neural lineage-related genes when cells, plasmid, and neural genes were loaded within the bio-ink to undergo gene transfection. It is noteworthy that the rheological properties of the bio-ink affect the cell reprogramming efficiency. It is also shown that a narrow processing window of shear stress (190 Pa) is optimal for transfection. In a separate study on the inkjet printing of Chinese Hamster Ovary Cells, it was shown that these transient pores recover within hours with no adverse effect on cell viability.[150] Both cases used shear force from bioprinting as a tool

for inducing physical responses to cells, adding the value to bioprinting being more than just material deposition.

Through selecting bio-ink that responds to stimuli, external forces can be applied during the printing process to induce heterogeneous material patterning. For instance, in a setup of a multi-nozzle extrusion printing system, a rotating magnet was positioned such that magnetic platelets within the printed ink were aligned to the external magnetic field.[151] An optical setup was also integrated to the system to induce the photocuring of the ink, fixing the oriented platelets to a specific direction. The printed construct displayed controlled heterogeneity in the microstructure. Patterned photomasks were used to selectively cure areas for controlled texturing. With the control over the microstructural architecture in the printed construct, the swelling and mechanical properties of the crosslinked polymers can be controlled, whereas constructs can be designed with programmable features.

D. Leveraging design-centric fabrication for better biomimicry

Other than inducing microstructural changes in the material through the printing process, the ability to bioprint multi-materials allow spatial control over the placement of these materials. For instance, heterogeneity in the collagen organization of the native skin tissue was recaptured through the use of polyvinylpyrrolidone (PVP)-based bio-ink to induce macromolecular crowding (MMC) within printed collagen layers.[70,152] The presence of PVP macromolecules alters the collagen fibrillogenesis process. With the precise control of PVP droplets within each printed collagen layer the fabrication of 3D hierarchical porous cell-laden printed collagen constructs is facilitated. The use of the defined compression approach has also been reported to generate gradients in the density and fibril morphology along the construct thickness.[153] The recent use of MMC for biological systems has attracted wide attention due to its ability to enhance extracellular matrix deposition and cell proliferation.[154,155]

In other native tissues, the cellular alignment is attributed to direction-dependent mechanical properties. From the mechanical and electrical properties of the heart[156] to the multinucleation of muscle fibres in myotube formation for musculoskeletal tissues,[157] there is a need to induce cell alignment in these engineered tissues. Through designing peripherals in the bioprinting setup, the design-based approach can be used to influence the biological behavior of printed constructs. For instance, customized printhead aligns cells by presenting a grooved surface for cells to grow along.[158]

To produce bioprinted constructs with mechanical properties resembling native tissue, bioprinting was integrated with non-bioprinting technologies. This provides a greater design freedom, hence controlling the mechanical properties of bioprinted constructs. For instance, Zhang and co-workers bioprinted urethra with mechanical properties matching the native tissue.[159] While cell-laden hydrogels deliver heterogeneous cells (urothelial cells and smooth muscle cells) in a well-distributed manner, thermoplastic scaffolds provide the structural and mechanical characteristics for the construct. Printed in different topological configurations, the spiral design of thermoplastic frames better mimics the mechanical properties of urethra as opposed to cylindrical design.

The automated assembly of pre-formed cell-containing units, termed as bioassembly,[160] is another field of technology that can be integrated with bioprinting. These bioassembly techniques include processes such as pick and place of spheroids and magnetic bioprinting with spatial control.[161–164] These microtissues are first cultured in specific conditions and assembled in modules. The culturing process allows the microtissues to mature prior to direct manipulation. The

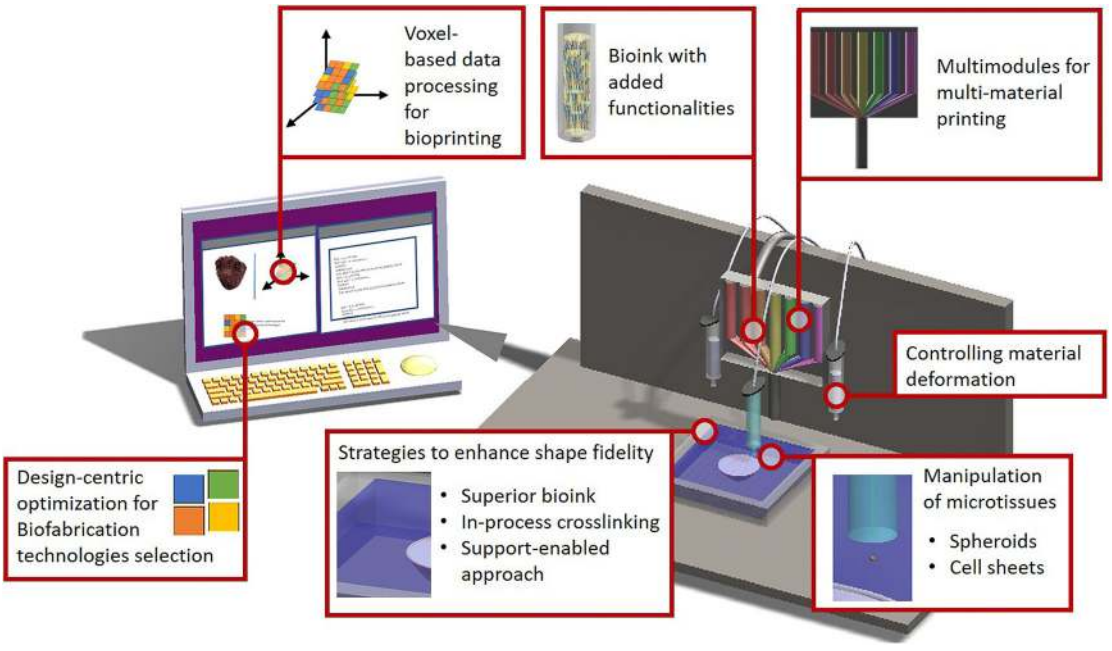

FIG. 7. Schematic illustration on fabricating complex tissues and organs using the multitude of pre-printing and printing technologies.

direct manipulation of these microtissues combined with bioprinting can potentially fabricate constructs with higher hierarchical complexity (Fig. 7).

IV. CONCLUSION

The ability to spatially control material and cell deposition has been well documented for bioprinting. In the pursuit of improving print resolution and accuracy, the principles behind each bioprinting technology were analyzed and categorized based on the fundamental units of filaments and droplets. These units correspond to material extrusion and material jetting techniques, respectively. On the other hand, vat photopolymerization may prove to be a technique that can fabricate engineered tissue at higher resolution. With each printing technology having different working principles, the definition of printability differs across variants of bioprinting. A guideline for printability evaluation is to determine whether the fundamental units can be achieved specific to the bioprinting technology. Another aspect on resolution is the cell distribution within the printed construct. Ensuring homogeneous cell distribution in the loading cartridge and the positioning of cells within each printed hydrogel will reduce the randomization of cell distribution in the printed tissue.

The ability to control material deposition in the vertical aspect determines the success of forming a three dimensionally defined construct. Several approaches can help improve the shape fidelity of the bioprinted construct. Formulating bio-ink with desirable rheological properties ensures that the material has sufficient mechanical properties to be self-supported. Introducing crosslinking agents at different printing stages helps us to retain the shape throughout the bioprinting process. Hydrogels with weaker mechanical properties are printed into desired forms through the use of supporting agents. Such supports may include changing the medium in which materials are deposited into and integrating bioprinting with mechanically robust thermoplastics. These strategies aim at improving the overall form of printed tissue.

Innovations at different stages of the bioprinting process will help to increase the functionalities of the bioprinted construct. Designing the blueprint for bioprinting will determine the degree of complexity of printed tissues. The voxel-based approach, where information for printing is represented by its fundamental units, will have better representation on the heterogeneity of the native tissue. Functionalities can be added to the engineered construct through formulating bio-inks that undergo predefined changes when exposed to external stimulation. The mechanical force from the bioprinting process can be leveraged to induce mechanical and biological responses in the printed construct. It is essential to understand that requirements and considerations vary with different types of tissues. The integration of bioprinting with different fabrication techniques can assist in capturing the different hierarchical attributes of a native tissue.

ACKNOWLEDGMENTS

This research was supported by the National Research Foundation, Prime Minister's Office, Singapore, under its Medium-Sized Centre funding scheme.

REFERENCES

[1]J. M. Lee, M. Zhang, and W. Y. Yeong, Microfluid. Nanofluid. **20**(1), 1–15 (2016).
[2]S. V. Murphy and A. Atala, Nat. Biotechnol. **32**(8), 773–785 (2014).
[3]J. M. Lee and W. Y. Yeong, Adv. Healthcare Mater. **5**(22), 2856–2865 (2016).
[4]M. Hospodiuk, M. Dey, D. Sosnoski, and I. T. Ozbolat, Biotechnol. Adv. **35**(2), 217–239 (2017).
[5]A. Arslan-Yildiz, R. El Assal, P. Chen, S. Guven, F. Inci, and U. Demirci, Biofabrication **8**(1), 014103 (2016).
[6]K. Kang, L. Hockaday, and J. Butcher, Biofabrication **5**(3), 035001 (2013).
[7]E. Y. S. Tan and W. Y. Yeong, Int. J. Bioprint. **1**, 49–56 (2015).
[8]J. M. Lee, S. L. Sing, M. Zhou, and W. Y. Yeong, Int. J. Bioprint. **4**(2), 151 (2018).
[9]W. L. Ng, J. M. Lee, W. Y. Yeong, and M. Win Naing, Biomater. Sci. **5**(4), 632–647 (2017).
[10]D. J. Odde and M. J. Renn, Trends Biotechnol. **17**(10), 385–389 (1999).
[11]A. Abeyewickreme, A. Kwok, J. R. McEwan, and S. N. Jayasinghe, Integr. Biol.-UK **1**(3), 260–266 (2009).
[12]Y. Fang, J. P. Frampton, S. Raghavan, R. Sabahi-Kaviani, G. Luker, C. X. Deng, and S. Takayama, Tissue Eng., Part C **18**(9), 647–657 (2012).
[13]T. Xu, W. Zhao, J. M. Zhu, M. Z. Albanna, J. J. Yoo, and A. Atala, Biomaterials **34**(1), 130–139 (2013).
[14]F. Guillemot, B. Guillotin, A. Fontaine, M. Ali, S. Catros, V. Keriquel, J. C. Fricain, M. Remy, R. Bareille, and J. Amedee-Vilamitjana, MRS Bull. **36**(12), 1015–1019 (2011).
[15]W. Lee, V. Lee, S. Polio, K. Fischer, J.-H. Lee, J. Park, and S.-S. Yoo, paper presented at the International Conference on Solid-State Sensors, Actuators and Microsystems, TRANSDUCERS 2009, pp. 2230–2233.
[16]H. Wijshoff, Curr. Opin. Colloid Interface Sci. **36**, 20–27 (2018).
[17]A. Muhammad, P. Emeline, D. Alexandre, F. Aurelien, and G. Fabien, Biofabrication **6**(4), 045001 (2014).
[18]F. Guillemot, A. Souquet, S. Catros, and B. Guillotin, Nanomedicine **5**(3), 507–515 (2010).
[19]D. Young, R. C. Y. Auyeung, A. Piqué, D. B. Chrisey, and D. D. Dlott, Appl. Surf. Sci. **197-198**, 181–187 (2002).
[20]J. T. Delaney, P. J. Smith, and U. S. Schubert, Soft Matter **5**(24), 4866–4877 (2009).
[21]J. Yan, Y. Huang, C. Xu, and D. B. Chrisey, J. Appl. Phys. **112**(8), 083105 (2012).
[22]D. Jang, D. Kim, and J. Moon, Langmuir **25**(5), 2629–2635 (2009).
[23]Z. Du, Y. Lin, R. Xing, X. Cao, X. Yu, and Y. Han, Polymer **138**, 75–82 (2018).
[24]A. Blaeser, D. F. D. Campos, U. Puster, W. Richtering, M. M. Stevens, and H. Fischer, Adv. Healthcare Mater. **5**(3), 326–333 (2016).
[25]B. Guillotin, A. Souquet, S. Catros, M. Duocastella, B. Pippenger, S. Bellance, R. Bareille, M. Rémy, L. Bordenave, and J. Amédée, Biomaterials **31**(28), 7250–7256 (2010).
[26]M. Gruene, A. Deiwick, L. Koch, S. Schlie, C. Unger, N. Hofmann, I. Bernemann, B. Glasmacher, and B. Chichkov, Tissue Eng., Part C **17**(1), 79–87 (2011).
[27]F. Guillemot, A. Souquet, S. Catros, B. Guillotin, J. Lopez, M. Faucon, B. Pippenger, R. Bareille, M. Rémy, S. Bellance, P. Chabassier, J. C. Fricain, and J. Amédée, Acta Biomater. **6**(7), 2494–2500 (2010).
[28]X. B. Chen, Int. J. Adv. Manuf. Technol. **43**(3), 276–286 (2009).
[29]M. G. Li, X. Y. Tian, and X. B. Chen, Biofabrication **1**(3), 032001 (2009).
[30]S. Ahn, H. Lee, and G. Kim, Carbohydr. Polym. **98**(1), 936–942 (2013).
[31]T. Billiet, E. Gevaert, T. De Schryver, M. Cornelissen, and P. Dubruel, Biomaterials **35**(1), 49–62 (2014).
[32]N. E. Fedorovich, H. M. Wijnberg, W. J. Dhert, and J. Alblas, Tissue Eng., Part A **17**(15–16), 2113–2121 (2011).
[33]Y. Huang, K. He, and X. Wang, Mater. Sci. Eng., C **33**(6), 3220–3229 (2013).
[34]H. Lee, S. Ahn, L. J. Bonassar, W. Chun, and G. Kim, Tissue Eng., Part C Methods **19**(10), 784–793 (2013).
[35]I. T. Ozbolat, H. Chen, and Y. Yu, Rob. Comput.-Integr. Manuf. **30**(3), 295–304 (2014).
[36]J.-H. Shim, J.-S. Lee, J. Y. Kim, and D.-W. Cho, J. Micromech. Microeng. **22**(8), 085014 (2012).
[37]J. E. Snyder, Q. Hamid, C. Wang, R. Chang, K. Emami, H. Wu, and W. Sun, Biofabrication **3**(3), 034112 (2011).

[38]X. H. Wang, Y. N. Yan, Y. Q. Pan, Z. Xiong, H. X. Liu, B. Cheng, F. Liu, F. Lin, R. D. Wu, R. J. Zhang, and Q. P. Lu, Tissue Eng. **12**(1), 83–90 (2006).
[39]B. Duan, L. A. Hockaday, K. H. Kang, and J. T. Butcher, J. Biomed. Mater. Res. Part A **101**(5), 1255–1264 (2013).
[40]A. Skardal, J. Zhang, and G. D. Prestwich, Biomaterials **31**(24), 6173–6181 (2010).
[41]J. Visser, B. Peters, T. J. Burger, J. Boomstra, W. J. Dhert, F. P. Melchels, and J. Malda, Biofabrication **5**(3), 035007 (2013).
[42]M. Müller, E. Öztürk, Ø. Arlov, P. Gatenholm, and M. Zenobi-Wong, Ann. Biomed. Eng. **45**(1), 210–223 (2017).
[43]M. Li, X. Tian, D. J. Schreyer, and X. Chen, Biotechnol. Prog. **27**(6), 1777–1784 (2011).
[44]W. Liu, M. A. Heinrich, Y. Zhou, A. Akpek, N. Hu, X. Liu, X. Guan, Z. Zhong, X. Jin, and A. Khademhosseini, Adv. Healthcare Mater. **6**(12), 1601451 (2017).
[45]J. A. Reid, P. A. Mollica, G. D. Johnson, R. C. Ogle, R. D. Bruno, and P. C. Sachs, Biofabrication **8**(2), 025017 (2016).
[46]N. Paxton, W. Smolan, T. Bock, F. Melchels, J. Groll, and T. Jungst, Biofabrication **9**(4), 044107 (2017).
[47]A. Skardal, M. Devarasetty, H.-W. Kang, I. Mead, C. Bishop, T. Shupe, S. J. Lee, J. Jackson, J. Yoo, S. Soker, and A. Atala, Acta Biomater. **25**, 24–34 (2015).
[48]R. Suntornnond, E. Y. S. Tan, J. An, and C. K. Chua, Materials **9**(9), 756 (2016).
[49]J. Gohl, K. Markstedt, A. Mark, K. Hakansson, P. Gatenholm, and F. Edelvik, Biofabrication **10**(3), 034105 (2018).
[50]O. Liliang, Y. Rui, Z. Yu, and S. Wei, Biofabrication **8**(3), 035020 (2016).
[51]W. Schuurman, P. A. Levett, M. W. Pot, P. R. V. Weeren, W. J. A. Dhert, D. W. Hutmacher, F. P. W. Melchels, T. J. Klein, and J. Malda, Macromol. Biosci. **13**(5), 551–561 (2013).
[52]J. H. Y. Chung, S. Naficy, Z. Yue, R. Kapsa, A. Quigley, S. E. Moulton, and G. G. Wallace, Biomater. Sci. **1**(7), 763–773 (2013).
[53]T. Gao, G. J. Gillispie, J. S. Copus, P. R. A. Kumar, Y. J. Seol, A. Atala, J. J. Yoo, and S. J. Lee, Biofabrication **10**(3), 034106 (2018).
[54]P. Soman, P. H. Chung, A. P. Zhang, and S. C. Chen, Biotechnol. Bioeng. **110**(11), 3038–3047 (2013).
[55]W. Zhu, X. Qu, J. Zhu, X. Ma, S. Patel, J. Liu, P. Wang, C. S. E. Lai, M. Gou, Y. Xu, K. Zhang, and S. Chen, Biomaterials **124**, 106–115 (2017).
[56]R. Gauvin, Y.-C. Chen, J. W. Lee, P. Soman, P. Zorlutuna, J. W. Nichol, H. Bae, S. Chen, and A. Khademhosseini, Biomaterials **33**(15), 3824–3834 (2012).
[57]V. B. Morris, S. Nimbalkar, M. Younesi, P. McClellan, and O. Akkus, Ann. Biomed. Eng. **45**(1), 286–296 (2017).
[58]S. Beke, F. Anjum, H. Tsushima, L. Ceseracciu, E. Chieregatti, A. Diaspro, A. Athanassiou, and F. Brandi, J. R. Soc., Interface **9**(76), 3017–3026 (2012).
[59]B. Busetti, B. Steyrer, B. Lutzer, R. Reiter, and J. Stampfl, Addit. Manuf. **21**, 413–421 (2018).
[60]W. Zhang and S. Chen, MRS Bull. **36**(12), 1028–1033 (2011).
[61]A. K. Nguyen and R. J. Narayan, Mater. Today **20**(6), 314–322 (2017).
[62]P. J. Bártolo, *Stereolithography* (Springer, 2011), pp. 1–36.
[63]M. Layani, X. F. Wang, and S. Magdassi, Adv. Mater. **30**(41), 1706344 (2018).
[64]Y. Luo, C. K. Dolder, J. M. Walker, R. Mishra, D. Dean, and M. L. Becker, Biomacromolecules **17**(2), 690–697 (2016).
[65]S. Sakai, H. Kamei, T. Mori, T. Hotta, H. Ohi, M. Nakahata, and M. Taya, Biomacromolecules **19**(2), 672–679 (2018).
[66]M. P. Lee, G. J. T. Cooper, T. Hinkley, G. M. Gibson, M. J. Padgett, and L. Cronin, Sci. Rep. **5**, 9875 (2015).
[67]D. Han, Z. Lu, S. A. Chester, and H. Lee, Sci. Rep. **8**(1), 1963 (2018).
[68]S. L. Khoon, L. Riccardo, F. C. Pedro, D. C. Miguel, R. A.-O. Cesar, M. A. v D. Kim, P. W. M. Ferry, G. Debby, J. H. Gary, M. Jos, and B. F. W. Tim, Biofabrication **10**(3), 034101 (2018).
[69]Z. Wang, X. Jin, Z. Tian, F. Menard, J. F. Holzman, and K. Kim, Adv. Healthcare Mater. **7**(9), 1701249 (2018).
[70]W. L. Ng, M. H. Goh, W. Y. Yeong, and M. W. Naing, Biomater. Sci. **6**(3), 562–574 (2018).
[71]W. L. Ng, W. Y. Yeong, and M. W. Naing, Materials **10**(2), 190 (2017).
[72]T. Mao, D. Kuhn, and H. Tran, AIChE J. **43**(9), 2169–2179 (1997).
[73]Z. Du, R. Xing, X. Cao, X. Yu, and Y. Han, Polymer **115**, 45–51 (2017).
[74]M. Duocastella, M. Colina, J. M. Fernández-Pradas, P. Serra, and J. L. Morenza, Appl. Surf. Sci. **253**(19), 7855–7859 (2007).
[75]Z. Zhang, R. Xiong, D. T. Corr, and Y. Huang, Langmuir **32**(12), 3004–3014 (2016).
[76]W. L. Ng, W. Y. Yeong, and M. W. Naing, Int. J. Bioprinting **2**(1), 53–62 (2016).
[77]W. L. Ng, W. Y. Yeong, and M. W. Naing, Procedia CIRP **49**, 105–112 (2016).
[78]W. Zongjie, A. Raafa, P. Benjamin, S. Roya, G. Sanjoy, and K. Keekyoung, Biofabrication **7**(4), 045009 (2015).
[79]J. L. Curley, S. R. Jennings, and M. J. Moore, J. Vis. Exp. **11**(48), 2636 (2011).
[80]C. X. Xu, M. Zhang, Y. Huang, A. Ogale, J. Z. Fu, and R. R. Markwald, Langmuir **30**(30), 9130–9138 (2014).
[81]P. S. Gungor-Ozkerim, I. Inci, Y. S. Zhang, A. Khademhosseini, and M. R. Dokmeci, Biomater. Sci. **6**, 915 (2018).
[82]W. L. Ng, S. Wang, W. Y. Yeong, and M. W. Naing, Trends Biotechnol. **34**(9), 689–699 (2016).
[83]M. N. Shahid, M. Amir, S. Mohamadmahdi, W. Philipp, G. Yuan, Z. Y. Shrike, D. Farideh, W. Wesley, A. Karen, M. C. Jonathan, K. Ali, and S. Su Ryon, Biofabrication **9**(1), 015020 (2017).
[84]M. E. Pepper, V. Seshadri, T. C. Burg, K. J. Burg, and R. E. Groff, Biofabrication **4**(1), 011001 (2012).
[85]J. Jia, D. J. Richards, S. Pollard, Y. Tan, J. Rodriguez, R. P. Visconti, T. C. Trusk, M. J. Yost, H. Yao, and R. R. Markwald, Acta Biomater. **10**(10), 4323–4331 (2014).
[86]B. Dersoir, M. R. de Saint Vincent, M. Abkarian, and H. Tabuteau, Microfluid. Nanofluid. **19**(4), 953–961 (2015).
[87]Z. B. Sendekie and P. Bacchin, Langmuir **32**(6), 1478–1488 (2016).
[88]K. Dubbin, Y. Hori, K. K. Lewis, and S. C. Heilshorn, Adv. Healthcare Mater. **5**(19), 2488–2492 (2016).
[89]C. A. Parzel, M. E. Pepper, T. Burg, R. E. Groff, and K. J. Burg, J. Tissue Eng. Regener. Med. **3**(4), 260–268 (2009).
[90]D. Chahal, A. Ahmadi, and K. C. Cheung, Biotechnol. Bioeng. **109**(11), 2932–2940 (2012).
[91]U. Demirci and G. Montesano, Lab a Chip **7**(9), 1139–1145 (2007).
[92]J. P. Lata, F. Guo, J. Guo, P.-H. Huang, J. Yang, and T. J. Huang, Adv. Mater. **28**(39), 8632–8638 (2016).
[93]C. W. Peak, J. Stein, K. A. Gold, and A. K. Gaharwar, Langmuir **34**(3), 917–925 (2018).
[94]Z. Wu, X. Su, Y. Xu, B. Kong, W. Sun, and S. Mi, Sci. Rep. **6**, 24474 (2016).
[95]S. Hong, D. Sycks, H. F. Chan, S. Lin, G. P. Lopez, F. Guilak, K. W. Leong, and X. Zhao, Adv. Mater. **27**(27), 4035–4040 (2015).
[96]V. H. M. Mouser, F. P. W. Melchels, J. Visser, W. J. A. Dhert, D. Gawlitta, and J. Malda, Biofabrication **8**(3), 035003 (2016).
[97]F. P. W. Melchels, W. J. A. Dhert, D. W. Hutmacher, and J. Malda, J. Mater. Chem. B **2**(16), 2282–2289 (2014).
[98]J. Yin, M. Yan, Y. Wang, J. Fu, and H. Suo, ACS Appl. Mater. Interfaces **10**(8), 6849–6857 (2018).
[99]M. Kesti, M. Müller, J. Becher, M. Schnabelrauch, M. D'Este, D. Eglin, and M. Zenobi-Wong, Acta Biomater. **11**, 162–172 (2015).
[100]K. Na, S. Shin, H. Lee, D. Shin, J. Baek, H. Kwak, M. Park, J. Shin, and J. Hyun, J. Ind. Eng. Chem. **61**, 340–347 (2018).
[101]C. Xu, W. Lee, G. Dai, and Y. Hong, ACS Appl. Mater. Interfaces **10**(12), 9969–9979 (2018).
[102]A. Forget, A. Blaeser, F. Miessmer, M. Köpf, D. F. D. Campos, N. H. Voelcker, A. Blencowe, H. Fischer, and V. P. Shastri, Adv. Healthcare Mater. **6**(20), 1700255 (2017).
[103]Y. Jin, C. Liu, W. Chai, A. Compaan, and Y. Huang, ACS Appl. Mater. Interfaces **9**(20), 17456–17465 (2017).
[104]W. Zhu, H. Cui, B. Boualam, F. Masood, E. Flynn, R. D. Rao, Z. Y. Zhang, and L. G. Zhang, Nanotechnology **29**(18), 185101 (2018).
[105]T. Kamperman, S. Henke, A. V. D. Berg, S. R. Shin, A. Tamayol, A. Khademhosseini, M. Karperien, and J. Leijten, Adv. Healthcare Mater. **6**(3), 1600913 (2017).
[106]L. Riccardo, V. Jetze, A. P. Josep, E. Elisabeth, M. Jos, and A. M.-T. Miguel, Biofabrication **6**(3), 035020 (2014).

[107]L. A. Hockaday, K. H. Kang, N. W. Colangelo, P. Y. Cheung, B. Duan, E. Malone, J. Wu, L. N. Girardi, L. J. Bonassar, H. Lipson, C. C. Chu, and J. T. Butcher, Biofabrication **4**(3), 035005 (2012).
[108]Q. Gao, Y. He, J-z Fu, A. Liu, and L. Ma, Biomaterials **61**, 203–215 (2015).
[109]Y. Nishiyama, M. Nakamura, C. Henmi, K. Yamaguchi, S. Mochizuki, H. Nakagawa, and K. Takiura, J. Biomech. Eng. **131**(3), 035001 (2008).
[110]O. Liliang, B. H. Christopher, B. R. Christopher, S. Wei, and B. A. Jason, Adv. Mater. **29**(8), 1604983 (2017).
[111]Y. B. Lee, S. Polio, W. Lee, G. Dai, L. Menon, R. S. Carroll, and S. S. Yoo, Exp. Neurology **223**(2), 645–652 (2010).
[112]A. Skardal, D. Mack, E. Kapetanovic, A. Atala, J. D. Jackson, J. Yoo, and S. Soker, Stem Cells Transl. Med. **1**(11), 792–802 (2012).
[113]Y. S. E. Tan and W. Y. Yeong, in *Proceeding of the 1st International Conference on Progress in Additive Manufacturing* (2014), 423–427.
[114]C. Li, A. Faulkner-Jones, A. R. Dun, J. Jin, P. Chen, Y. Xing, Z. Yang, Z. Li, W. Shu, D. Liu, and R. R. Duncan, Angew. Chem., Int. Ed. **54**(13), 3957–3961 (2015).
[115]S. Sakai, K. Ueda, E. Gantumur, M. Taya, and M. Nakamura, Macromol. Rapid Commun. **39**(3), 1700534 (2018).
[116]K. Arai, Y. Tsukamoto, H. Yoshida, H. Sanae, T. A. Mir, S. Sakai, T. Yoshida, M. Okabe, T. Nikaido, and M. Taya, Int. J. Bioprint. **2**(2), 153–162 (2016).
[117]S. Sakai, K. Hirose, K. Taguchi, Y. Ogushi, and K. Kawakami, Biomaterials **30**(20), 3371–3377 (2009).
[118]S. Sakai, Y. Yamada, T. Zenke, and K. Kawakami, J. Mater. Chem. **19**(2), 230–235 (2009).
[119]T. J. Hinton, Q. Jallerat, R. N. Palchesko, J. H. Park, M. S. Grodzicki, H.-J. Shue, M. H. Ramadan, A. R. Hudson, and A. W. Feinberg, Sci. Adv. **1**(9), e1500758 (2015).
[120]W. Wu, A. DeConinck, and J. A. Lewis, Adv. Mater. **23**(24), H178 (2011).
[121]A. Blaeser, D. F. D. Campos, M. Weber, S. Neuss, B. Theek, H. Fischer, and W. Jahnen-Dechent, BioRes. Open Access **2**(5), 374–384 (2013).
[122]A. D. Graham, S. N. Olof, M. J. Burke, J. P. K. Armstrong, E. A. Mikhailova, J. G. Nicholson, S. J. Box, F. G. Szele, A. W. Perriman, and H. Bayley, Sci. Rep. **7**(1), 7004 (2017).
[123]Y. Jin, W. Chai, and Y. Huang, Mater. Sci. Eng.: C **80**, 313–325 (2017).
[124]D. B. Kolesky, R. L. Truby, A. S. Gladman, T. A. Busbee, K. A. Homan, and J. A. Lewis, Adv. Mater. **26**(19), 3124–3130 (2014).
[125]J. S. Miller, K. R. Stevens, M. T. Yang, B. M. Baker, D.-H. T. Nguyen, D. M. Cohen, E. Toro, A. A. Chen, P. A. Galie, X. Yu, R. Chaturvedi, S. N. Bhatia, and C. S. Chen, Nat. Mater. **11**(9), 768–774 (2012).
[126]S. Wüst, M. E. Godla, R. Müller, and S. Hofmann, Acta Biomater. **10**(2), 630–640 (2014).
[127]A. Skardal, J. Zhang, L. McCoard, X. Xu, S. Oottamasathien, and G. D. Prestwich, Tissue Eng., Part A **16**(8), 2675–2685 (2010).
[128]H.-W. Kang, S. J. Lee, I. K. Ko, C. Kengla, J. J. Yoo, and A. Atala, Nat. Biotechnol. **34**(3), 312–319 (2016).
[129]R. Levato, W. R. Webb, I. A. Otto, A. Mensinga, Y. Zhang, M. van Rijen, R. van Weeren, I. M. Khan, and J. Malda, Acta Biomater. **61**, 41–53 (2017).
[130]M. Kesti, C. Eberhardt, G. Pagliccia, D. Kenkel, D. Grande, A. Boss, and M. Zenobi-Wong, Adv. Funct. Mater. **25**(48), 7406–7417 (2015).
[131]C. P. Radtke, N. Hillebrandt, and J. Hubbuch, J. Chem. Technol. Biotechnol. **93**(3), 792–799 (2018).
[132]W. Schuurman, V. Khristov, M. W. Pot, P. R. van Weeren, W. J. Dhert, and J. Malda, Biofabrication **3**(2), 021001 (2011).
[133]J. H. Shim, J. Y. Kim, M. Park, J. Park, and D. W. Cho, Biofabrication **3**(3), 034102 (2011).
[134]F. Pati, J. Jang, D.-H. Ha, S. Won Kim, J.-W. Rhie, J.-H. Shim, D.-H. Kim, and D.-W. Cho, Nat. Commun. **5**, 3935 (2014).
[135]R. Suntornnond, E. Y. S. Tan, J. An, and C. K. Chua, Sci. Rep. **7**(1), 16902 (2017).
[136]T. Xu, K. W. Binder, M. Z. Albanna, D. Dice, W. Zhao, J. J. Yoo, and A. Atala, Biofabrication **5**(1), 015001 (2013).
[137]M. S. Mannoor, Z. Jiang, T. James, Y. L. Kong, K. A. Malatesta, W. O. Soboyejo, N. Verma, D. H. Gracias, and M. C. McAlpine, Nano Lett. **13**(6), 2634–2639 (2013).
[138]B. Duan, E. Kapetanovic, L. A. Hockaday, and J. T. Butcher, Acta Biomater. **10**(5), 1836–1846 (2014).
[139]X.-Y. Yang, L.-H. Chen, Y. Li, J. C. Rooke, C. Sanchez, and B.-L. Su, Chem. Soc. Rev. **46**(2), 481–558 (2017).
[140]C. Bader, D. Kolb, J. C. Weaver, S. Sharma, A. Hosny, J. Costa, and N. Oxman, Sci. Adv. **4**(5), eaas8652 (2018).
[141]L. Wanjun, Z. Y. Shrike, H. A. Marcel, F. De Fabio, J. H. Lin, B. S. Mahwish, A. M. Moisés, Y. Jingzhou, L. Yi-Chen, T. D. S. Grissel, M. A. K. Z. Kai, K. Parastoo, P. Gyan, C. Hao, G. Xiaofei, Z. Zhe, J. Jie, Z. G. Harry, J. Xiangyu, S. S. Ryon, D. M. Remzi, and K. Ali, Adv. Mater. **29**(3), 1604630 (2017).
[142]Y. Y. Ling, T. Y. S. Edgar, T. H. K. Joel, P. Z. Kai, L. X. Yi, Y. W. Yee, T. C. S. Hui, and L. Augustinus, Rapid Prototyping J. **23**(2), 227–235 (2017).
[143]S. J. Lee, T. Esworthy, S. Stake, S. Miao, Y. Y. Zuo, B. T. Harris, and L. G. Zhang, Adv. Biosyst. **2**(4), 1700213 (2018).
[144]S. Agarwala, J. M. Lee, W. L. Ng, M. Layani, W. Y. Yeong, and S. Magdassi, Biosens. Bioelectron. **102**, 365–371 (2018).
[145]M. Shevach, S. Fleischer, A. Shapira, and T. Dvir, Nano Lett. **14**(10), 5792–5796 (2014).
[146]S. Wang, J. M. Lee, and W. Y. Yeong, Int. J. Bioprint. **1**(1), 3–14 (2015).
[147]A. M. Kloxin, A. M. Kasko, C. N. Salinas, and K. S. Anseth, Science **324**(5923), 59–63 (2009).
[148]A. S. Gladman, E. A. Matsumoto, R. G. Nuzzo, L. Mahadevan, and J. A. Lewis, Nat. Mater. **15**(4), 413 (2016).
[149]L. Ho and S-h Hsu, Acta Biomater. **70**, 57–70 (2018).
[150]X. Cui, D. Dean, Z. M. Ruggeri, and T. Boland, Biotechnol. Bioeng. **106**(6), 963–969 (2010).
[151]D. Kokkinis, M. Schaffner, and A. R. Studart, Nat. Commun. **6**, 8643 (2015).
[152]W. L. Ng, J. T. Z. Qi, W. Y. Yeong, and M. W. Naing, Biofabrication **10**(2), 025005 (2018).
[153]T. Novak, B. Seelbinder, C. M. Twitchell, C. C. van Donkelaar, S. L. Voytik-Harbin, and C. P. Neu, Adv. Funct. Mater. **26**(16), 2617–2628 (2016).
[154]A. Satyam, P. Kumar, X. Fan, A. Gorelov, Y. Rochev, L. Joshi, H. Peinado, D. Lyden, B. Thomas, and B. Rodriguez, Adv. Mater. **26**(19), 3024–3034 (2014).
[155]R. Rashid, N. S. J. Lim, S. M. L. Chee, S. N. Png, T. Wohland, and M. Raghunath, Tissue Eng., Part C **20**(12), 994–1002 (2014).
[156]M. Papadaki, N. Bursac, R. Langer, J. Merok, G. Vunjak-Novakovic, and L. E. Freed, Am. J. Physiol. **280**(1), H168–H178 (2001).
[157]P. M. Wigmore and G. F. Dunglison, Int. J. Dev. Biol. **42**(2), 117–125 (1998); available at http://www.ncbi.nlm.nih.gov/pubmed/9551857.
[158]X. Shi, S. Ostrovidov, Y. Zhao, X. Liang, M. Kasuya, K. Kurihara, K. Nakajima, H. Bae, H. Wu, and A. Khademhosseini, Adv. Funct. Mater. **25**(15), 2250–2259 (2015).
[159]K. Zhang, Q. Fu, J. Yoo, X. Chen, P. Chandra, X. Mo, L. Song, A. Atala, and W. Zhao, Acta Biomater. **50**(Supplement C), 154–164 (2017).
[160]G. Jürgen, B. Thomas, B. Torsten, A. B. Jason, C. Dong-Woo, D. D. Paul, D. Brian, F. Gabor, L. Qing, A. M. Vladimir, M. Lorenzo, N. Makoto, S. Wenmiao, T. Shoji, V. Giovanni, B. F. W. Tim, X. Tao, J. Y. James, and M. Jos, Biofabrication **8**(1), 013001 (2016).
[161]V. Mironov, Y. D. Khesuani, E. A. Bulanova, E. V. Koudan, V. A. Parfenov, A. D. Knyazeva, A. N. Mitryashkin, N. Replyanski, V. A. Kasyanov, and F. Pereira D.A.S, Int. J. Bioprint. **2**(1), 8 (2016).
[162]C. Norotte, F. S. Marga, L. E. Niklason, and G. Forgacs, Biomaterials **30**(30), 5910–5917 (2009).
[163]G. Ludwig, K. Sabrina, T. Kevin, B. Leo, F. Günter, Z. Roland, K. Peter, G. B. Stark, and Z. Stefan, Biofabrication **9**(2), 025027 (2017).
[164]A. M. Blakely, K. L. Manning, A. Tripathi, and J. R. Morgan, Tissue Eng., Part C **21**(7), 737–746 (2015).